RSC Advances

ROYAL SOCIETY
OF CHEMISTRY

www.rsc.org/advances

DNA/protein interaction, cytotoxic activity and magnetic properties of amino-alcohol Schiff base derived Cu(II)/Ni(II) metal complexes: Influence of the nuclearity and metal ions

Meiju Niu [a][*], Zhen Li [a], Huanhuan Li [a], Xiao Li [a], Jianmin Dou [a], Suna Wang [a][*]

[a] *Shandong Provincial Key Laboratory of Chemical Energy Storage and Novel Cell Technology, School of Chemistry and Chemical Engineering, Liaocheng University, Liaocheng, 252059, P. R. China*

Abstract. Four coordination complexes based on two amino-alcohol derived Schiff base ligands, namely, $[Cu(H_2L^1)(Cl)]$ CH_3OH (**1**), $[Cu_4((HL^2)_2(H_2L^2)_2(H_2O)(C_2H_5OH)]$ $2(ClO_4)$ $2(C_2H_5OH)$ (**2**), $[Ni_2(H_2L^1)_2(OAc)_2(C_2H_5OH)_2]_2$ (**3**) and $[Ni_4(HL^2)_3(\mu_3\text{-}O)(H_2O)_3]$ $9H_2O$ (**4**) (H_3L^1 = {2-ethyl-2-((2-hydroxybenzylideneamino)propane-1,3-diol, and H_3L^2 = 2-ethyl-2-((2-hydroxy-3-methoxybenzylideneamino)propane-1,3-diol), were synthesized and characterized. Alkoxo and phenoxo groups of the Schiff base ligands bridge the metal atoms in diverse modes, leading to interesting mononuclear (**1**), dinuclear (**3**), and tetranuclear (**2** and **4**) complexes, respectively. The *in vitro* cytotoxic effect of these complexes on cancerous cell lines, including human lung carcinoma cell line (A549), human colon carcinoma cell lines (HCT-116), human promyelocytic leukemia cells (HL-60) and chronic myelogenous leukemia cells line (K-562) showed that all these complexes exhibited substantial cytotoxic activity. Their interactions with calf thymus DNA (CT-DNA) and bovine serum albumin (BSA) were also investigated using UV-visible, fluorescence and synchronous fluorescence spectroscopic methods. All complexes could quench the intrinsic fluorescence of BSA in a static quenching process. Variable temperature magnetic properties of these complexes were investigated in details. The nuclearity and metal centers play an important role on the properties of the complexes.

Keywords: Amino-alcohol Schiff base; Crystal structure; Anticanter activities;

 [*] Corresponding author 👤 ✉ . Tel: +86 0635 8230615; Fax: +86 0635 8239121.
E-mail address: niumeiju@163.com, wangsuna@lcu.edu.cn
Shandong Provincial Key Laboratory of Chemical Energy Storage and Novel Cell Technology
School of Chemistry and Chemical Engineering
Liaocheng University Liaocheng 252059
P. R. China

Magnetic properties

1. Introduction

Recent years have witnessed the rapid development of polynuclearity complexes, stemming not only from their fascinating molecular architectures but also their applications, including catalysis, fluorescence, non-linear optics, gas storage, magnetism as well as biological activity, and so on. [1-2] Control of the construction and properties of these complexes is largely dependent on the choice of both metal centers and organic ligands.

Since the discovery of the anti-proliferate properties of *cis*-platin by Rosenberg et al., anticancer activities of such kinds of metal complexes have been intensely investigated in recent decades. [2a] And much effort has also been extended to non-platinum metal-based agents. A number of transition-metal complexes, such as Cu(II), Zn(II) and Ni(II), have been reported. These metals play a significant role in biological systems and have been reported as potential anticancer agents both active in vitro and in vivo. Their complexes based upon diverse ligands, such as thiosemicarbazone [6], quinolinoline and substituted quinolinoline [7], and other N-donor heterocyclic ligands [8], could exhibit anticancer activities. It is well-known that many complexes exert their drug effects through binding to DNA or proteins. Investigation of the interactions of these complexes with DNA or proteins is basic and crucial to design and discover more-efficacious, target-specific, less-toxic drugs. DNA offers a variety of binding sites and binding modes for non-covalent interactions with metal complexes, such as electrostatic interactions, groove binding and intercalation. Bovine serum albumin (BSA), in the meantime, is often chosen as a target protein for the study of interactions with small molecules because of its low cost, ready availability and similarity to human serum albumin. Their interactions with complexes could be reflected by various techniques, especially spectroscopic methods, including UV-visible (UV-Vis), fluorescence, circular dichroism (CD), and so on.

We have been recently focused on designing novel amino-alcohol ligands and investigating their self-assembly with metal centers, as well as properties of corresponding complexes. [9] Herein, two amino-alcohol ligands, namely {2-ethyl-2-((2-hydroxybenzylideneamino)propane-1,3-diol (**H₃L^1**), and 2-ethyl-2-((2-hydroxy-3-methoxybenzylideneamino)propane-1,3-diol (**H₃L^2**) (Scheme 1), were synthesized. And based on these ligands, four coordination complexes,

namely, $[Cu(H_2L^1)(Cl)] \, CH_3OH$ **(1)**,

$[Cu_4((HL^2)_2(H_2L^2)_2(H_2O)(C_2H_5OH)] \, 2(ClO_4) \, 2(C_2H_5OH)$ **(2)**,

$[Ni_2(H_2L^1)_2(OAc)_2(C_2H_5OH)_2]_2$ **(3)** and $[Ni_4(HL^2)_3(\mu_3\text{-}O)(H_2O)_3] \, 9H_2O$ **(4)**, were obtained. Alkoxo and phenoxo groups of the Schiff base ligands bridge metal atoms in diverse modes, leading to interesting mononuclear (**1**), dinuclear (**3**), and tetranuclear (**2** and **4**) complexes, respectively. The *in vitro* cytotoxic effect of these complexes on cancerous cell lines, including human lung carcinoma cell line (A549), human colon carcinoma cell lines (HCT-116), human promyelocytic leukemia cells (HL-60) and chronic myelogenous leukemia cells line (K-562) showed that all these complexes exhibited substantial cytotoxic activity. Their interactions with calf thymus DNA (CT-DNA) and bovine serum albumin (BSA) were also investigated using UV-visible, CD and fluorescence spectroscopic methods. All complexes could quench the intrinsic fluorescence of BSA in a static quenching process. The overall order of interaction between these four complexes and CT-DNA as well as BSA decreased in the order **2** > **4** > **3** > **1**. The results indicated that the nuclearity and metals have large influence on the anticancer activities. Variable temperature magnetic properties of these complexes were investigated in details.

2. Experimental Section

2.1 Materials

All reagents and solvents were purchased from commercial sources and used without further purification. The Schiff base ligands, **H₃L¹** and **H₃L²** had been synthesized in our laboratory as described as the literature. [10] The ligands were prepared by refluxing salicylaldehyde or 3-methoxysalicylaldehyde with 2-amino-2-ethyl-1,3-propanediol for 4h, respectively. The resulting yellow solutions of the ligands **H₃L¹** and **H₃L²** were subsequently isolated as crystalline solids.

***Caution!** Perchlorate salts are potentially explosive. Only a small amount of the materials should be prepared and handled with care.*

Synthesis of $[Cu(H_2L^1)Cl] \, CH_3OH$ (1)

A methanolic solution of $CuCl_2 \, 2H_2O$ (0.170 g, 1 mmol) was added to the methanol solution of **H₃L¹** (0.2233 g, 1 mmol). The mixture was stirred at room temperature for 4 h and then filtered. Blue block crystals of **1** were obtained by slow evaporation of the methanol solution after a few days. Yield: 71.2%. M. p.: 152-154 ℃. $C_{13}H_{20}CuClNO_4$ (M$_r$=353.29): *Anal*. Calc. (%) C, 49.35; H, 5.18; N, 3.59%. Found: C,

49.58; H, 5.46; N, 3.76%. Selected IR (KBr pellet: cm^{-1}): 3352 (s), 1626 (m), 1180(m), 623 (m), 509 (m), 474 (m).

Synthesis of [Cu$_4$((HL^2)$_2$(H$_2$L^2)$_2$(H$_2$O)(C$_2$H$_5$OH)] 2(ClO$_4$) 2(C$_2$H$_5$OH) (2)

An ethanolic solution of Cu(ClO$_4$)$_2$ 6H$_2$O (0.3705 g, 1 mmol) was added to the ethanolic solution of **H$_3$L^2** (0.2533 g, 1 mmol). The mixture was stirred at room temperature for 4 h and then filtered. Blue rod-shaped crystals of **2** were obtained by slow evaporation of the solution after several days. Yield: 68.5%. M. p.: 154-157 ℃. C$_{58}$H$_{88}$Cu$_4$Cl$_2$N$_4$O$_{28}$ (M$_r$=1614.38): *Anal*. Calc. (%) C, 43.15; H, 5.49; N, 3.47%. Found: C, 43.39; H, 5.61; N, 3.23%. Selected IR (KBr pellet: cm^{-1}): 3422(s), 1641 (m), 1137 (m), 1080 (s), 673 (m), 480 (m).

Synthesis of [Ni$_2$(H$_2$L^1)$_2$(OAc)$_2$(C$_2$H$_5$OH)$_2$]$_2$ (3)

An ethanolic solution of Ni(OAc)$_2$ 4H$_2$O (0.2488 g, 1 mmol) was added to the ethanol solution of **H$_3$L^1** (0.2233 g, 1 mmol). The mixture was stirred at room temperature for 4 h and then filtered. Green block crystals of **3** were obtained by slow evaporation of the ethanol solution after two weeks. Yield: 75.3%. M. p.: 249-252 ℃. C$_{32}$H$_{50}$Ni$_2$N$_2$O$_{12}$ (M$_r$=772.16): *Anal*. Calc. (%) C, 49.78; H, 6.53; N, 3.63%. Found: C, 49.59; H, 6.76; N, 3.72%. Selected IR (KBr pellet: cm^{-1}): 3396 (s), 1635 (m), 1599 (s), 1337 (s), 623 (m), 522 (m).

Synthesis of [Ni$_4$(HL^2)$_3$(μ_3-O)(H$_2$O)$_3$] 9H$_2$O (4)

A methanolic solution of Ni(NO$_3$)$_2$ 6H$_2$O (0.2908 g, 1 mmol) was added to the methanol solution of **H$_3$L^2** (0.2533 g, 1 mmol). The mixture was stirred at room temperature for 4 h and then filtered. Green block crystals of **4** were obtained by slow evaporation of the methanol solution after several weeks. Yield: 76.2%. M. p. 294-297 ℃. C$_{39}$H$_{84}$Ni$_4$N$_3$O$_{31}$ (M$_r$=1325.86): *Anal*. Calc. (%) C, 35.33; H, 6.39; N, 3.17%. Found: C, 35.23; H, 6.31; N, 3.10%. Selected IR (KBr pellet: cm^{-1}): 3443 (s), 1634 (m), 1159 (m), 624 (m), 545 (m).

2.2 Physical measurements

The melting points were obtained with an X-4 digital micro melting-point apparatus and were uncorrected. The IR spectra (4000-400 cm^{-1}) were recorded on a Nicolet-5700 spectrophotometer with KBr pellets. Elemental analyses (C, H, N) were carried out by a Perkin Elmer-2400 II elemental analyzer. Electronic absorption spectra were recorded using a HP-8453A diode array spectrophotometer. Emission spectra were measured with LS55 spectrofluorometer. Circular dichroism (CD) spectra measurements were measured on a Jasco J-810 spectropolarimeter. Magnetic

susceptibility measurements were performed using a Quantum Design SQUID VSM magnetometer. All data were corrected for diamagnetism estimated from Pascal's constants.[11]

2.3 Crystal Data Collection and Refinement

Diffraction data for the complexes were collected at 298K on a Bruker SMART 1000 CCD area detector equipped with graphite-monochromated Mo $K\alpha$ radiation (λ = 0.71073 Å). Empirical absorption corrections were applied using the SADABS program. [12] The structures were solved by the direct method and refined by the full-matrix least-squares method on F^2 using SHELXS 97 and SHELXL 97 programs, respectively. All non-hydrogen atoms were refined with anisotropic thermal parameters. [13] The hydrogen atoms attached to carbon atoms were placed in calculated positions and refined using the riding model. For complex **2**, perchlorate anions show disorder and some restraints were applied. For complex **4**, the solvent aqua molecules are highly disordered, and attempts to locate and refine them were unsuccessful. The SQUEEZE program was used to remove scattering from the highly disordered solvent molecules. [14] The structure was solved by using the new generated .HKL file. A summary of the crystallographic data and refinement parameters for the complexes are provided in Table 1. Selected bond lengths and angles are listed in Table 2. CCDC-918246 (**1**), 918249 (**2**), 918247 (**3**) and 918248 (**4**) contain the supplementary crystallographic data for this paper. These data can be obtained free of charge from The Cambridge Crystallographic Data Center via http://www.ccdc.cam.ac.uk.

3. Results and discussion

3.1 Description of the structures

$[Cu(H_2L^1)Cl]\ CH_3OH\ (1)$

Complex **1** crystallizes in Orthorhombic space group *Pna*2$_1$ and consists of an independent mononuclear unit (Figure 1a). The Cu1 center is four-coordinated with one imine nitrogen atom (N1), one phenolic oxygen atom (O2) and one undeprotonated alkoxo-oxygen atom (O1) from the Schiff base ligand and one chlorine atom (Cl1), affording a square-planar coordination geometry with the maximum deviation of 0.0258(30) Å for N1 from the least-squares plane, in which the Schiff base ligand (H_3L^1) acts as a bivalent negatively tridentate NOO chelating mode with free -CH$_2$OH group. These bond angles fall in the normal range of 82.1(3)-95.1(3) °, respectively, which are consistent with those reported previously for

the copper analogue. [15] It was observed that the phenyl ring C(2)-C(7) and the six-membered ring C(1)-C(2)-C(7)-N(1)-O(2)-Cu(1) are almost coplanar with a small dihedral angle of ca. 5.36 °, suggesting an electron delocalization over the ligand. [16]

As shown in Figure S1a in Supporting Information, 1-D polymeric chain is formed by weak Cu ··Cl interactions between the mononuclear units along *a* axis with the Cu(1)-Cl(1)-Cu(1)[#] angle of 98.59 ° and the Cl1 ··Cu1[#] (symmetry code: 0.5+x, 1.5-y, z) distance of 2.970 Å, which is longer than that in other complexes. [17] These polymeric chains are further reinforced by strong hydrogen-bonding interactions O3-H3 ··O2 between the neighboring mononuclear molecules. The H-bonds parameters are presented in Table S2 in Supporting Information.

$[Cu_4(HL^2)_2(H_2L^2)_2(H_2O)(C_2H_5OH)]$ $2(ClO_4)$ $2(C_2H_5OH)$ (2)

Complex **2** crystallizes in Triclinic space group *P*-1 and consists of a discrete $[Cu_4(HL^2)_2(H_2L^2)_2]$ tetramer, with an L/M molar ratio of 4:4. The four potentially tetradentate Schiff base ligands (H_3L^2) exhibit different coordination modes: two coordinating in a tetradentate form $[\mu_3:\eta^1:\eta^1:\eta^3-(HL^2)^{2-}]$ through one imino nitrogen, one μ_2-phenoxo, one deprotonated alkoxo-oxygen and one methoxy oxygen atom which bridges two copper(II) centers; the other two coordinating in a tridentate form $[\mu_2:\eta^2:\eta^3-(HL^2)^-]$ through one imino nitrogen, one phenoxo and one deprotonated μ_3-alkoxo oxygen atom which bridges three copper(II) centers, thus affording a boat-shaped Cu_4O_4 unit (Figure 1b). The remaining neutral alkoxyl group -CH_2OH is left non-coordinated.

Cu1 and Cu3 centers are six-coordinated with one imino nitrogen atom and five oxygen atoms from Schiff-base ligands, adopting a distorted octahedral coordination sphere. While Cu2 and Cu4 centers are five-coordinated with one imino nitrogen atom and three oxygen atoms from Schiff-base ligands, making up the basal plane of square-pyramidal geometry and the oxygen atom from ethanol (for Cu2) or water molecule (for Cu4) locating at the vertex of the square-pyramid. Obviously, the axial Cu-O bond lengths [2.292(5)-2.654(5) Å] are much longer than the equatorial Cu-O lengths [1.898(5)-2.041(4) Å] due to the Jahn-Teller effect of an octahedral Cu(II) ion with a d^9 electron configuration. The displacements of copper centers from their mean basal plane are 0.0464(25) Å for Cu1, 0.0206(28) Å for Cu2, 0.1503(26) Å for Cu3, and 0.1079(25) Å for Cu4, respectively.

Four copper(II) centers in the boat-shaped Cu_4O_4 unit occupy alternate cubane vertices, and the tetranuclear structure can be viewed as two Cu_2O_2 dimers joined

together by weak Cu-O bridges, with the intradimeric Cu1··Cu4 [3.2585(14)Å] and Cu2··Cu3 [3.2655(9)Å] distances shorter than the interdimeric Cu··Cu [3.3186(12)-3.7532(14)Å] distances. The two short and four long Cu··Cu distances in the Cu_4O_4 core can be classified as the relatively rare "2+4" class defined by Ruiz and co-workers. [18] The Cu-O-Cu angles are in the range of 89.41(4)-120.28(1)°. Interestingly, weak intradimeric hydrogen bonds are observed between the coordinated aqua or ethanol molecule and the coordinated phenoxo groups (O17-H17B··O1 for $Cu1Cu4O_2$ dimer and O18-H18··O9 for $Cu2Cu3O_2$ dimer), which might be the reason of the short distance between intradimeric metal centers. [19]

The 2-D honeycomb-like supramolecular structure was formed by intermolecular hydrogen bonding interactions between the free -CH_2OH groups [O4-H4··O16 (symmetry code: x-1, y, z) and O8-H8··O11 (symmetry code: x+1, y-1, z)]. In addition, perchlorate anions are enclosed within the structure through the feeble C-H··O interaction and compensate the positive charge (Figure S2 in Supporting Information). The H-bonds parameters are presented in Table S2 in Supporting Information.

$[Ni_2(H_2L^1)_2(OAc)_2(C_2H_5OH)_2]_2$ (3)

Complex **3** crystallizes in Triclinic space group *P*-1 and the asymmetry unit comprised of two crystallographically independent binuclear nickel molecules (named **A** and **B**, respectively) with the Ni_2O_2 units in which two symmetry-related Ni centers are doubly bounded together by two μ_2-phenolic oxygen atoms of the partly deprotonated ligands (Figure 2a). The two binuclear nickel molecules are isostructural and only molecule **A** is described representatively. In **A**, the Ni1 center is six-coordinated with one imine nitrogen (N1), one protonated alkoxo (O1) and two symmetry-related phenolic oxygen atoms (O3, O3^i) of the Schiff-base ligand (H_2L^1), one monodentate acetic oxygen atom (O4) and one alcohol oxygen atom (O6), affording a distorted octahedral coordination geometry with the atoms N1, O1, O3 and O3^i on the equatorial plane. The deviation of Ni1 from the equatorial plane is 0.025 Å (while 0.042 Å for Ni2) and the *cis* and *trans* angles of the atoms in the equatorial plane vary from 84.44(12) to 96.76(13)° and 172.89(12) to 168.94(12)°, respectively (Table S1 in Supporting Information).The elongated axial bond lengths of Ni1-O4 and Ni1-O6 in **A**, which caused by Jahn-Teller distortion, are 2.072(3) Å and 2.167(3) Å. Within each binuclear, the doubly bridged metal centers are separated with the Ni··Ni distance of 3.106 Å and 3.098 Å, respectively. And the Ni-O-Ni

angles are 99.23(1) and 98.26(3) °, respectively.

Weak intermolecular hydrogen bonds [O2-H2···O11, 2.799(4) Å, 170.5° and O8-H8···O5, 2.759(4) Å, 169.2°] were observed between the neighboring molecules **A** and **B**, forming a 1-D chain running along c axis. Then, the honeycomb-like shaped structure (Figure S3 in Supporting Information) was formed through the weak C30-H30A···O8 hydrogen contacts between neighboring 1-D chains. The H-bonds parameters are presented in Table S2 in Supporting Information.

[Ni$_4$(HL^2)$_3$(μ_3-O)(H$_2$O)$_3$] 9H$_2$O (4)

Complex **4** also has a M$_4$O$_4$ cubane core. It crystallizes in cubic space group P-4$_3$n and comprising of a discrete [Ni$_4$(HL^2)$_3$(μ_3-O)(H$_2$O)$_3$] tetramer with an L^2/M molar ratio of 3:4 (Figure 2b). In the tetramer, each (HL^2)$^{2-}$ ligand coordinates with three nickel atoms (Ni1, Ni1 and Ni2) in a tetradentate mode. Four Ni(II) ions are held together by three deprotonated μ_3-alkoxo oxygen atoms [O3, O3^i and O3^{ii} (symmetry codes: i, x, -y+1, -z+1; ii, -x+1, y, -z+1.) and one μ_3-O^{2-} anion, forming a Ni$_4$O$_4$ cubane core. Within this core, there are three equivalent Ni1 atoms and one crystallographically independent Ni2 atom. Ni1 center is six-coordinated with one imine nitrogen atom N1, one phenolic oxygen atom O1, and two symmetry-related μ_3-alkoxo oxygen atoms (O3, O3^i) of the Schiff-base ligand (L^2)$^{2-}$, one coordinated water molecule (O13) and one dianionic μ_3-oxygen anion (O5^{2-}), forming a distorted octahedral coordination geometry with the displacement of 0.0470(51) Å for Ni1 from the equatorial plane defined by the atoms N1, O1, O3 and O5. The Ni2 center is also six-coordinated with a centrosymmetric *trans*-octahedral environment furnished by six oxygen atoms belonging to the hydroxyl groups from three deprotonated Schiff base ligands, with the Ni-O distances of 2.035(8) Å for O3, O3^i and O3^{ii} and 2.116(8) Å for O8, O8^i and O8^{ii}, respectively (Table S1 in Supporting Information). The intracluster Ni···Ni distances of Ni1···Ni2 and Ni1^i···Ni1 are 3.053(2) and 3.088(3) Å, respectively. All the doubly bridged Ni-O-Ni angles are in the range of 94.41(3)-97.42(2) °.

The neighboring tetramers are associated into 3-D supramolecular net (Figure S4 in Supporting Information) through the C-H···π interactions between benzene carbon atom (C5) and the neighboring benzene ring [3.58(3) Å, 143.5°]. The H-bonds parameters are presented in Table S2 in Supporting Information.

3.2 Magnetic properties

Variable temperature magnetic susceptibility measurements for complexes **2-4** were

measured on polycrystalline samples with the temperature range of 1.8–300 K and an applied magnetic field of 1kOe. The $\chi_M T$ and χ_M^{-1} vs. T plots for all complexes are shown in Figure 3.

As shown in Figure 3a, the value of $\chi_M T$ of complex **2** at 300 K is 1.48 cm^3 K mol^{-1}, compared with the value of 1.5 cm^3 K mol^{-1} for four spin-only Cu(II) ions (S = 1/2, g = 2.0). Upon cooling, $\chi_M T$ decreases steadily, indicating an overall antiferromagnetic coupling between the Cu(II) ions. The low values at low temperatures suggested a spin ground state S = 0. Taking into account the boat-shaped tetranuclear structure, the corresponding network of exchange pathways is shown in Scheme 2a. The pathways of these interactions could be classified into three types: (i) J_1, through one alkoxido bridge (Cu1 ··Cu2 and Cu3 ··Cu4); (ii) J_1, through one alkoxido and one phenoxido bridge (Cu1 ··Cu4 and Cu2 ··Cu3) and (iii) J_3, through two alkoxido bridges (Cu1 ··Cu3). Considering the long distance of Cu1-O12 (2.578(4) Å) and Cu3-O3 (2.654(4) Å). Cu1 ··Cu3 magnetic exchange should be small and may be negligible. Accordingly, this system could be analyzed as a ring with antiferromagnetic interactions between neighboring Cu(II) ions. The Heisenberg spin Hamiltonian was written as: H = -2$J_1(S_1S_2+S_3S_4)$-2$J_2(S_1S_4+S_2S_3)$. Considering the similar pathways, we simplified the problem by considering $J_1 = J_2$, and obtained the best fits with $J_1 = J_2$ = -22.8(2) cm^{-1} and g = 2.12. The similar treatment has been observed in the similar boat-shaped Cu$_4$ compound. [20]

For complex **3**, the value of $\chi_M T$ at room temperature is 2.48 cm^3 K mol^{-1}, consistent with the expected value (2.4 cm^3 K mol^{-1}) for two spin-only Ni(II) ions with g = 2.20 (Figure 3b). With the temperature decreases, the $\chi_M T$ gradually increases and reach a maximum of 2.78 cm^3 K mol^{-1} at about 23 K, suggesting possible weak ferromagnetic exchange between Ni(II) ions. Below this temperature, the value of $\chi_M T$ falls rapidly to 1.95 cm^3 K mol^{-1} at 1.8 K, which may be attributed to the weak inter-molecular antiferromagnetic interactions and/or zero-field splitting as well as Zeeman effects. [11] Considering the weak interactions between adjacent binuclear cores, only the intrabinuclear coupling interactions are taken into account. The data were fitted assuming the isotropic spin-coupling Hamiltonian (H = -2JS_1S_2) and zero-field splitting (D), and intermolecular interaction (zJ'). [21] The optimized magnetic data were: J = 4.58 cm^{-1}, zJ' = 0.015cm^{-1}, g = 2.25, D = 5.58 cm^{-1}.

The $\chi_M T$ value of complex **4** is equal to 5.40 cm^3 K mol^{-1}, much larger than the expected value for four spin-only S = 1 Ni(II) centers with g = 2.20 (4.84 cm^3 K mol^{-1})

(Figure 3c). Upon cooling, $\chi_M T$ continuously increases and reaches a maximum of 16.11 cm^3 K mol^{-1}at 32 K, indicating dominant ferromagnetic interactions between the Ni(II) ions. And then the value of $\chi_M T$ quickly decreases and reaches 7.49 cm^3 K mol^{-1} at 1.8 K, probably due to weak intermolecular antiferromagnetic interactions attributed to the inter-molecular antiferromagnetic interactions, and/or zero-field splitting as well as Zeeman effects. Similarly, only the coupling interactions between the four Ni(II) centers within the cubane core were considered (Scheme 2b): (a) J_1, through two alkoxido bridges (Ni2 ··Ni1, Ni2 ··Ni1^i, and Ni2 ··Ni1^{ii}); and (b) J_2, through one alkoxido and one oxygen anion bridges (Ni1 ··Ni1^i, Ni1 ··Ni1^{ii}, and Ni1^i ··Ni1^{ii}). The Heisenberg spin Hamiltonian was written as: $H = -2J_1(S_1S_2+S_3S_4)-2J_2(S_1S_4+S_2S_3)$. The data were simulated by considering J_1 and J_2 are equal. The best fits were obtained only between the temperature above 40K with the following parameters: $J_1 = J_2 = 23.83$ cm^{-1} and $g = 2.25$.

The magneto-structural corrections for oxygen bridged Cu^{II} and Ni^{II} compounds have been well established. [20, 22] The coupling is largely dependent upon the M-O-M angles. Most of the Cu-O-Cu angles in complex **2** are in the range of 91-120°, which are responsibility of the antiferromagnetic interaction. For Ni complexes, the magnetic coupling is expected to be ferromagnetic when angles are close to 90°, and a change from ferromagnetic to antiferromagnetic exchange coupling corresponds to a Ni-O-Ni angle of about 98-99°. All Ni-O-Ni angles within complex **4** are in range of 94-97°. Other factors, including the Ni-O distances, the dihedral angles as well as the distortion of the coordination geometry, all have different influences on magnetic exchange coupling.

3.2 Cytotoxicity

In vitro cell culture studies are valuable tools for the screening of chemotherapy agents and provide preliminary data for further relative studies. The cytotoxicities of the complexes to different cells were evaluated through the loss of cell viability using MTT assay.[23] The effects of the complexes on the viability of these cells evaluated after an exposure period of 48 h showed antitumour activity and their corresponding IC_{50} values, related to inhibition of tumour cell growth at the 50% level, are shown in Table 2. The lower IC_{50} indicates that the cells are more sensitive to drugs and the inhibitory proliferation effect of the drugs on the cells is more obvious. The IC_{50} values against four cell lines A549, HCT-116, HL-60 and K-562 are shown in Table 2.

The inhibition effects of complexes **1**-**4** against the four cell lines at a concentration of 20.0μg/mL are listed in Figure 4. The experimental results indicated that the cytotoxicities are significantly dependent upon the structures of the complexes, including the metal centers and the nuclearity. Tetranuclear complex **2** is most significantly remarkable and displays all cytotoxicity against all tested four cell lines, especially HL-60 and A549. Other three complexes, however, exhibit selective cytotoxicity against different cell lines.

3.3 DNA-binding properties

In order to explore the relationship on structures, activities as well as the anticancer mechanism, further studies were performed on the interactions of complexes **1**-**4** with DNA and protein BSA through UV-Vis, fluorescent and synchronous fluorescence spectra as well as CD spectra.

The absorption spectra of complexes **1**-**4** in the absence and presence of CT-DNA are shown in Figure 5 (complex **3**) and Figure S5 in Supporting Information (complexes **1**, **2** and **4**). The strong absorption spectra at about 360 nm for all complexes may be assigned to the ligand-to-metal charge transfer (LMCT). With the increase of the concentration of DNA, all the adsorption bands showed hypochromism accompanied with bathochromic shifts, similar to those previously reported metallointercalators. [24] Generally, the complex could intercalate to the base pairs of DNA. And the π^* orbital of the intercalators may couple with the π orbital of the base pairs, decrease the π-π^* transition probabilities and consequently lead to hypochromism. As can be seen from the insert plot of Figure 5, -$[DNA]/(\varepsilon_a-\varepsilon_f)$ versus $[DNA]$ for complexes **1**-**4** all exhibit good linearity. The intrinsic binding constant K_b were calculated according to the equation [25]: $[DNA]/(\varepsilon_a-\varepsilon_f) = [DNA]/(\varepsilon_b-\varepsilon_f) + 1/K_b(\varepsilon_b-\varepsilon_f)$. $[DNA]$ is the concentration of DNA in base pairs, ε_a is the apparent extinction coefficient obtained by calculating $A_{obs}/[complex]$, ε_f corresponds to the extinction coefficient of the complex in its free form, and ε_b refers to the extinction coefficient of the complex in the bound form. The K_b values for these complexes were calculated to be 2.28×10^3, 1.35×10^4, 2.39×10^3 and 2.55×10^3 M^{-1}, respectively. The magnitude of the binding constant value indicated medium binding strength of the complex with CT-DNA.

Ethidium bromide (EB) is a planar organic cationic dye. Due to its strong intercalation between the adjacent DNA base pairs, it often emits intense fluorescent light in the presence of DNA. When EB bounded to DNA was replaced by metal

complexes, significant fluorescence quench may be observed because of the reduction of the number of binding sites on the DNA that is available to the EB. As a consequence, the competitive binding experiments using metal complexes as quenchers could provide some information about the binding of the complexes to DNA. This displacement method serves as an indirect evidence to identify intercalative binding modes. As illustrated in Figure 6 and Figure S6 in Supporting Information, when the concentrations of the complex increased, the intensity of the fluorescence spectra emission band at 590 nm of the EB-DNA system obviously decreased. Hence, these complexes may bind to CT-DNA with an intercalative mode. The plots of I_0/I vs r ($r = c_{VOL}/c_{DNA}$) exhibited a good linearity, suggesting the quenching of EB bound to DNA by the test complex is in good agreement with the linear Stern-Volmer equation. [26] The Stern-Volmer quenching constant, K_{sq}, for these complexes were 1.01, 1.69, 1.38 and 1.52, respectively. These values are higher than those for some other complexes. [27] And among the four complexes, strongest interactions were present between DNA and complex **2**.

To monitor the conformation of DNA in solution, Circular Dichrosim (CD) spectrum was performed. The CD spectrum of DNA exhibits a positive peak at 278 nm and a negative peak at 246 nm, respectively. The former is due to the base stacking and the latter to the helicity of B-type DNA. [28] As shown in Figure 7 and Figure S7 in Supporting Information, the intensities of two characteristic peaks of DNA in the presence of complexes **1**-**4** all decreased and the positions were slightly red-shifted, indicating the presence of binding interactions between DNA and complexes. These interactions may have effect on the $\pi\cdots\pi$ stacking interactions of DNA base pairs. Moreover, the interactions may be assigned to intercalation, consistent with UV and fluorescence spectra.

3.4 BSA-binding property

Generally, the fluorescence of a protein is caused by three intrinsic characteristics of the protein, namely tryptophan, tyrosine, and phenylalanine residues. Molecular interactions may reduce the fluorescence intensity, including excited-state reactions, molecular rearrangement, energy transfer ground-state complex formation and collision quenching. Consequently, fluorescence spectroscopy could be used to qualitatively analyze the binding of complexes to protein. BSA is selected as a target protein in our cases. As shown in Figure 8 and Figure S8 in Supporting Information, increase of the concentration of the complex leads to the decrease of the fluorescence

emission of BSA at 346 nm, indicating the formation of complex-BSA system. This quenching effect was also analyzed by the Stern-Volmer equation: $I_0/I = 1 + K_{sv}[Q]$, where I_0 and I are the fluorescence intensities of fluorophore at 346 nm in the absence and presence of complexes. $[Q]$ is the concentration of quencher and K_{sv} is the Stern-Volmer quenching constant. Fitting the linear plot of I_0/I versus $[Q]$ resulted the K_{sv} values for four complexes are 0.47×10^5, 1.43×10^5, 0.54×10^5 and 0.53×10^5 M^{-1}, respectively.

The fluorescence quenching could commonly be classified as two types: dynamic quenching and static quenching. The former is reduced by the interaction between the fluorophore and quencher, while the latter is related with the formation of a non-fluorescent complex by fluorophore and quencher. UV-Vis sorption spectra could be performed to differentiate these two quenching types. As illustrated in Figure 9 and Figure S9 in Supporting Information, BSA displays the absorption at 278 nm. Addition of the complex to BSA led to the enhancement of the intensity of the absorption with a slight red-shift. This result may suggest the presence of a static interaction between the complex and BSA due to the formation of a complex-BSA ground state system, which has been found in other reported samples. [24,29] That is, the fluorescent quenching may be ascribed to static quenching. For static quenching interaction, the apparent binding constant (equilibrium constant) K_b and the number of binding sites n could be obtained from the fluorescence data according to the Scatchard equation: $\log((I_0-I)/I) = \log K_b + n\log[Q]$.[30] A plot of $\log((I_0-I)/I)$ versus $\log[Q]$ for complexes **1**-**4** was shown in Figure 10 and the values were listed in Table 3. The value of n was approximately equal to 1, which indicated that there was only one class of independent binding sites for the complexes on BSA.

Synchronous fluorescence spectrum could also provide information on the molecular microenvironment. In synchronous fluorescence spectroscopy, the difference between excitation and emission wavelengths ($\Delta\lambda = \lambda_{em} - \lambda_{ex}$) reflects the spectra of a different nature of chromophores and the large $\Delta\lambda$ (60 nm, for example) and small $\Delta\lambda$ (15 nm, for example) values for BSA system are ascribed to the fluorescence of tryptophan and tyrosine residue, respectively. [29] We also measured synchronous fluorescence spectra in order to study the structural changes of BSA in the presence of different complexes. The synchronous fluorescence spectra were recorded at both $\Delta\lambda = 15$ and 60 nm, respectively. As shown in Figure 11 and Figure S10 in Supporting Information, when the concentration of complexes increased, the

fluorescence intensities decreased with a slight bathochromic shift for tyrosine emission while a slight hypsochromic shift for tryptophan emission. Accordingly, these complexes affected both the environments of tyrosine and tryptophan residues of BSA.

From all above measurements, one can see that complex **2** and **1** display the strongest and weakest interactions with both DNA and BSA, respectively, consistent with the cycrotoxicity. For complex **2**, the binding constant K_b for DNA and BSA was 1.35×10^4 and 6.91×10^5 M^{-1}, which is near to that of the classical intercalator EB (K_b, 3.3×10^5 M^{-1}). Therefore, the binding mode between the complex and DNA or BSA was classical intercalative.

All spectroscopic methods clearly proved that the overall order of interaction between these four complexes and CT DNA as well as BSA decreased in the order **2** > **4** > **3** > **1**. That is, among the four complexes, complex **2**, the tetranuclear copper complex, exhibited strongest binding with both DNA and BSA. This phenomena may be related with the presence of an electron donor group OCH$_3$ at the ortho- position of phenol hydroxyl with the presence of the coordination of this phenol hydroxyl group with Cu centers. The releasing nature of the group may assist the respective interactions between the complex and either DNA or protein. Similar phenomena have been observed in other complexes. [24]

Conclusions.

The reactions of amino-alcohol derived Schiff-base ligands with Cu(II) and Ni(II) salts have afforded four novel polynuclear complexes. The metal centers and nuclearity play an important role on the magnetic and cytotoxic properties of the complexes. Magnetic measurements indicated that antiferromagnetic and ferromagnetic magnetic coupling interactions were present within Cu(II) and Ni(II) complexes, respectively. From the bio-inorganic chemistry point of view, binding interactions of the four complexes with CT-DNA and BSA revealed that among the four complexes tetranulear Cu(II) complex showed the most significant effect on their binding ability, and tetranulear Ni(II) complex showed higher cytotoxicity and stronger binding ability than the dinuclear one. The exact molecular mechanism requires further detailed investigation.

Acknowledgment.

Shandong Province (ZR2013BM017 and ZR2012BQ023).

Supporting Information

Additional figures for crystal structures and properties of the complexes; Tables of selected bond lengths and angles, hydrogen-bonding parameters of the complexes.

References

1 (a) L. K. Thompson, O. Waldmann , Z. Q. Xu, *Coord. Chem. Rev.*, 2005, **249**, 2677; (b) H. Miyasaka, A. Saitoh, S. Abe, *Coord. Chem. Rev.*, 2007, **251**, 2622; (c) C. E. Kostakis, A.K. Powell, *Coord. Chem. Rev.*, 2009, **253**, 2686; (d) J. L. Liu, Y. C. Chen, F. S. Guo, M. L. Tong, *Coord. Chem. Rev.*, 2014, **281**, 26; (d) T. Taguchi, W. Wernsdorfer, K. A. Abboud, G. Christou, *Inorg. Chem.*, 2010, **49**, 199; (e) S. N. Wang, L. Q. Kong, H. Yang, Z. T. He, Z. Jiang, D. C. Li, S. Y. Zeng, M. J. Niu, Y. Song, J. M. Dou, *Inorg. Chem.*, 2011, **50**, 2705.

2 (a) B. Rosenberg, L. Van Camp, J. E. Trosko, V. H. Mansour, *Nature*, 1969, **222**, 385. (b) C. Santini, M. Pellei, V. Gandin, M. Porchia, F. Tisato. C. Marzano, *Chem. Rev.*, 2014, **114**, 815 and references therein; (c) W. K. Liu, R. Gust, *Chem. Soc. Rev.*, 2013, **42**, 755 and references therein; (d) S. Banerjee, E. B. Veale, C. M. Phelan, S. A. Murphy, G. M. Tocci, L. J. Gillespie, D. O. Frimannsson, J. M. Kelly, T. Gunnlaugasson, *Chem. Soc. Rev.*, 2013, **42**, 1601 and references therein; (e) G. Gasser, I. Ott, N. Metzler-Nolte, *J. Med. Chem.*, 2011, **54**, 3 and references therein; (f) H. K. Liu, P. J. Sadler, *Acc. Chem. Res.*, 2011, **44**, 349 and references therein; (g) J. A. Drewry, P. T. Gunning, *Coord. Chem. Rev.*, 2011, **255**, 459 and references therein.

3 (a) M. J. Li, T. Y. Lan, X. H. Cao, H. H. Yang, Y. Shi, C. Yi, G. N. Chen, *Dalton. Trans.*, 2014, **43**, 2789; (b) N. Pravin, N. Raman, *Eur. J. Med. Chem.*, 2014, **85**, 675. (c) N. P. E. Barry, P. J. Sadler, *Chem. Commun.*, 2013, **49**, 5106; (d) S. S. Bhat, A. A. Kumbhar, H. Heptullah, A. A. Khan, V. V. Gobre, S. P. Gejji, V. G. Puranik, *Inorg. Chem.*, 2011, **50**, 545; (e) S. Ramakrishnan, D. Shakthipriya, E. Suresh, V. S. Periasamy, M. A. Akbarsha, M. Palaniandavar, *Inorg. Chem.*, 2011, **50**, 6458; (f) F. Arjmand, F. Sayeed, M. Muddassir, *J. Photochem. Photobio. B.*, 2011, **103**, 166.

4 (a) M. O'Connor, A. Kellett, M. McCann, G. Rosair, M. McNamara, O. Howe, B. S. Creaven, S. McClean, A. Foltyn-Arfa Kia, D. O'Shea, M. Devereux, *J. Med. Chem.*,

2012, **55**, 1957; (b) P. Krishnamoorthy, P. Sathyadevi, R. R. Butorac, A. H. Cowley, N. S. P. Bhuvaneshc, N. Dharmaraj, *Dalton. Trans.*, 2012, **41**, 44236; (c) D. S. Raja, N. S. P. Bhuvanesh, K. Natarajan, *Eur. J. Med. Chem.*, 2011, **46**, 4584; (d) S. Ramakrishinan, D. Shakthipriya, E. Suresh, V. S. Periasamy, M. A. Akbarsha, M. Palaniandavar, *Inorg. Chem.*, 2011, **50**, 6458; (e) M. Nath, P. K. Saini, *Dalton. Trans.*, 2011, **40**, 7077.

5 (a) S. N. Georgiades, N. H. Abd Karim, K. Suntharalingam, R. Vilar, *Angew. Chem. Int. Ed.*, 2010, **49**, 4020; (b) F. Tisato, C. Marzano, M. Porchia, M. Pellei, C. Santini, *Med. Res. Rev.*, 2010, **30**, 708 and references therein; (c) P. C. A. Bruijnincx, P. J. Sadler, *Curr. Opin. Chem. Biol.*, 2008, **12**, 197; (d) M. C. Prabhakara, B. Basavaraju, H. S. Bhojya Naik, *Bioinorg. Chem. Appl.*, 2007, **2007**, 36497.

6 (a) J. Shao, Z. Y. Ma, A. Li, Y. H. Liu, C. Z. Xie, Z. Y. Qiang, J. Y. Xu, *J. Inorg. Biochem.*, 2014, **136**, 13; (b) A. Basu, D. Thiyagarajan, C. Kar, A. Ramesh, G. Das, *RSC Adv.*, 2013, **3**, 14088.

7 (a) K. B. Huang, Z. F. Chen, Y. C. Liu, M. Wang, J. H. Wei, X. L. Xie, J. L. Zhang, K. Hu, H. Liang, *Eur. J. Med. Chem.*, 2013, **70**, 640; (b) Y. C. Liu, J. H. Wei, Z. F. Chen, M. Liu, Y. Q. Gu, K. B. Huang, Z. Q. Li, H. Liang, *Eur. J. Med. Chem.*, 2013, **69**, 554.

8 (a) V. M. Manikandamathavan, T. Weyhermüller, R. P. Parameswari, M. Sathishkumar, V. Subramanian, B. U. Nair, *Dalton. Trans.*, 2014, **43**, 13018; (b) P. P. Silva, W. Guerra, G. C. dos Santos, N. G. Fernandes, J. N. Silveira, A. M. da Costa Ferreira, T. Bortolotto, H. Terenzi, A. J. Bortoluzzi, A. Neves, E. C. Pereira-Maia, *J. Inorg. Biochem.*, 2014, **132**, 67; (c) M. N. Noolvi, H. M. Patel, S. Kamboj, A. Kaur, V. Mann, *Eur. J. Med. Chem.*, 2012, **56**, 56; (d) S. Shuuha, A. Shah, Z. Rehman, N. Muhammad, S. Ali, R. Qureshi, N. Khalid, A. Meetsma, *Eur. J. Med. Chem.*, 2010, **45**, 2902.

9 (a) P. Li, M. J. Niu, M. Hong, S. Cheng and J. M. Dou, *J. Inorg. Biochem.*, 2014, **137**, 101; (b) P. Li, M. F. Niu, M. J. Niu, M. Hong, *Z. Anorg. Allg. Chem.*, 2014, **640**, 2238.

10 H. H. Li, M. J. Niu, D. W. Sun, S. N. Wang, S. Cheng, *Inorg. Chem. Commun.*, 2013, **27**, 97.

11 O. Kahn, *Molecular Magnetism*, 1993.

12 G. M. Sheldrick, Program for Empirical Absorption Correction of Area Detector

Data; University Göttingen, Göttingen, Germany, 1996.

13 G. M. Sheldrick, SHELXL-97 Program for Crystal Structure Refinement, Institut für Anorganische Chemie, University Göttingen, Göttingen, Germany, 1997.

14 A. L. Spek, *J. Appl. Crystallogr.*, 2003, **36**, 7.

15 H. Liu, F. Gao, D. Niu, J. Tian, *Inorg. Chim. Acta.*, 2009, **362**, 4179.

16 S. Shit, S. K. Dey, C. Rizzoli, E. Zangrando, G. Pilet, C. J. Gomez-Garcia, S. Mitra, *Inorg. Chim. Acta.*, 2011, **370**, 18.

17 W. E. Estes, W. E. Hatfield, J. A. C. van Ooijen, J. Reedijk, *J. Chem. Soc.*, *Dalton. Trans.*, 1980, 2121.

18 E. Ruiz, A. Rodrguez-Fortea, P. Alemany, S. Alvarez, *Polyhedron*, 2001, **20**, 1323.

19 (a) C. Ding, C. Gao, S. Ng, B. Wang and Y. Xie, *Chem. Eur. J.*, 2013, **19**, 9961; (b) A. Burkhardt, E. T. Spielberg, H. Gorls, W. Plass, *Inorg. Chem.*, 2008, **47**, 2485.

20 P. Bhowmik, N. Aliaga-Alcalde, V. Gómez, M. Corbella, S. Chattopadhyay, *Polyhedron*, 2013, **49**, 269.

21 H. Sakiyama, T. Suzuki, K. Ono, R. Ito, Y. Watanabe, M. Yamasaki, M. Mikuriya, *Inorg. Chim. Acta*, 2005, **358**, 1897.

22 (a) J. M. Clemente-Juan, E. Coronado, J. R. Galan-Mascaros, C. J. Gomez-Garcia, *Inorg. Chem.*, 1999, **38**, 55; (b) U. Kortz, Y. P. Jeannin, A. Teze, G. Herve, S. Isber, *Inorg. Chem.*, 1999, **38**, 3670; (c) P. Mukherjee, M. G. B. Drew, C. J. Gómez-García, A. Ghosh, *Inorg. Chem.*, 2009, **48**, 5848; (d) B. Biswas, U. Pieper, T. Weyhermuller, P. Chaudhuri, *Inorg. Chem.*, 2009, **48**, 6781.

23 M. Blagosklonny, W. S. EI-diery, *Int. J. Cancer*, 1996, **67**, 386.

24 P. Sathyadevi, P. Krishnamoorthy, R. R. Butorac, A. H. Cowley, N. S. P. Bhuvanesh, N. Dharmaraj, *Dalton. Trans.*, 2011, **40**, 9690.

25 A. Wolfe, G. H. Shimer and T. Meehan, *Biochemistry.*, 1987, **26**, 6392.

26 J. R. Lakowicz, G. Weber, *Biochemistry*, 1973, **12**, 4161.

27 (a) M. Baldini, M. Belicchi-Ferrari, F. Bisceglie, G. Pelosi, S. Pinelli, P. Tarasconi, *Inorg. Chem.*, 2004, **43**, 7170; (b) F. Wang, H. D. Yin, C. H. Yue, S. Cheng, M. Hong, *J. Organomet. Chem.*, 2013, **738**, 35.

28 (a) H. Y. Liu, L. Z. Li, Q. Guo, J. F. Dong, J. H. Li, *Transit. Met. Chem.*, 2013, **38**, 441; (b) A. Rajendran, B. U. Nair, *Biochim. Biophys. Acta.*, 2006, **1760**, 1794.

29 P. Krishnamoorthy, P. Sathyadevi, R. R. Butorac, A. H. Cowley, N. S. P. Bhuvaneshc, N. Dharmaraj, *Dalton. Trans.*, 2012, **41**, 4423.

30 Y. J. Hu, Y. Liu, J. B. Wang, X. H. Xiao, S. S. Qu, *J. Pharm. Biomed. Anal.*, 2014,

36, 915.

H_3L^1 R = H

H_3L^2 R = OCH$_3$
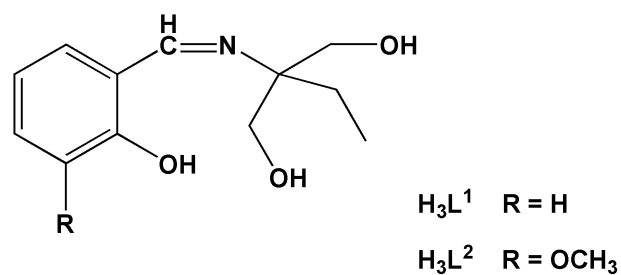
Scheme 1. View of the structures of two Schiff base ligands.

(a)   (b)
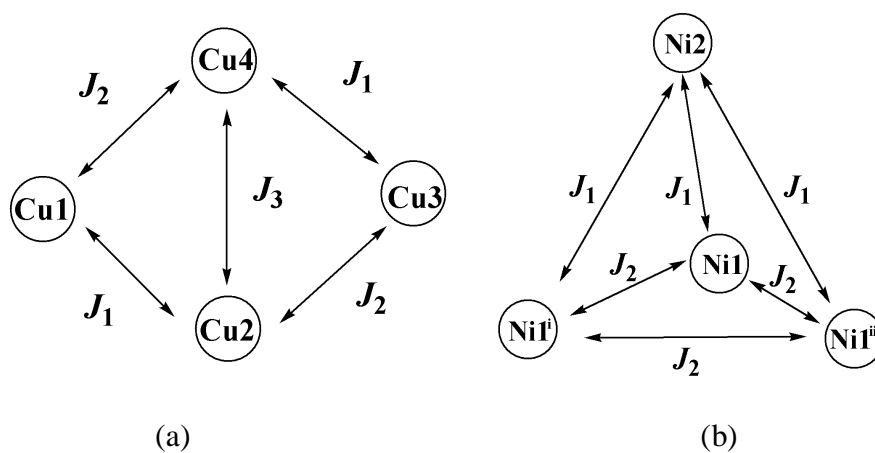
Scheme 2. Scheme representation of magnetic coupling interactions within the tetranuclear structures of complex **2** (a) and **4** (b), respectively.

Table 1. Crystal data collection and structure refinement parameters for complexes
1-4.

Complex	**1**	**2**	**3**	**4**
Formula	$C_{13}H_{20}ClCuNO_4$	$C_{58}H_{88}Cl_2Cu_4N_4O_{28}$	$C_{32}H_{50}N_2Ni_2O_{12}$	$C_{39}H_{84}N_3Ni_4O_{31}$
Formula weight	353.29	1614.38	772.16	1325.86
Crystal system	Orthorhombic	Triclinic	Triclinic	Cubic
space group	Pna2(1)	P-1	P-1	P-43n
a/Å	7.480(9)	13.6420(12)	10.2560(10)	23.4500(17)
b/Å	15.997(18)	13.8856(14)	11.9039(12)	23.4500(17)
c/Å	12.467(18)	21.048(2)	15.3331(16)	23.4500(17)
α/ °	90	89.928(2)	90.2240(10)	90
β/ °	90	81.7480(10)	97.4350(10)	90
γ/ °	90	62.5610(10)	104.270(2)	90
V/Å^3	1492(3)	1542.5(2)	1797.7(3)	12895.2(16)
Z	4	2	2	8
T/K	298(2)	298(2)	298(2)	298(2)
D_{calc}/g cm^{-3}	1.573	1.535	1.426	1.255
R_{int}	0.1300	0.0422	0.0255	0.0000
R_1,wR_2 [I>2σ(I)]	0.0676, 0.1605	0.0681, 0.1659	0.0447, 0.1060	0.0778, 0.2037
R^a(all data)	0.1095, 0.1968	0.1126, 0.1868	0.0821, 0.1313	0.1636, 0.2037
GOF	1.048	1.019	1.023	1.036

[a] $R_1=\sum (| F_o-F_c |)/\sum| F_o|$. $wR_2=\{\sum[w(| F_o-F_c |)^2]/\sum[w|Fo|^2]\}^{1/2}$

Table 2. IC$_{50}$ (μM) of all complexes against human lung carcinoma cell line (A-549), human colon carcinoma cell lines (HCT-116), human promyelocytic leukemia cells (HL-60) and chronic myelogenous leukemia cells (K-562) for 48 h treatment.

Cell lines	*cis*-platin	1	2	3	4
A-549	53	> 50	16.05	> 50	> 50
HCT-116	> 60	45.08	30.02	39.93	> 50
HL-60	> 60	23.50	13.17	27.15	38.55
K-562	> 60	17.76	27.28	> 50	42.63

Table 3. Comparison of interaction study results between complexes **1–4** on DNA and BSA.

Complex	DNA-binding		BSA-binding		
	K_{sq}	K_b (M^{-1})	K_{sv}(M^{-1})	K_b (M^{-1})	n
1	1.01	2.28×10^3	0.47×10^5	9.16×10^3	1.03
2	1.69	1.35×10^4	1.36×10^5	6.91×10^5	0.87
3	1.38	2.39×10^3	0.53×10^5	5.46×10^5	1.02
4	1.52	2.55×10^3	0.54×10^5	5.51×10^5	1.05

(a)

(b)
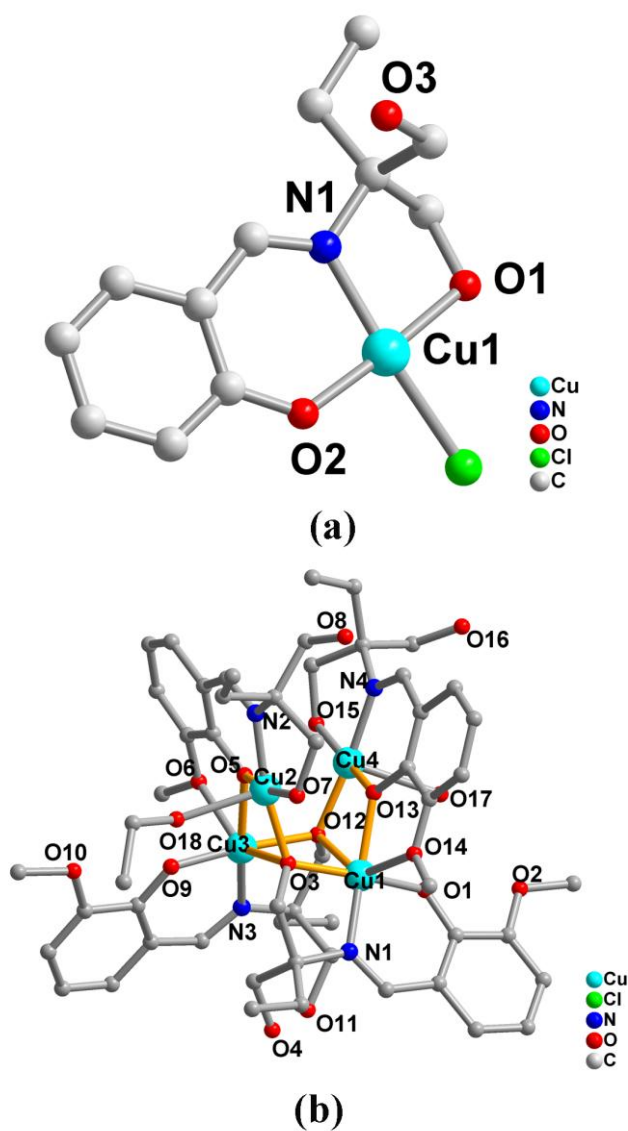
Figure 1. (a) The perspective view of mononuclear unit in complex **1**. Hydrogen atoms attached to carbon atoms are omitted for clarity. (b) The perspective view of boat-shaped $\{Cu_4O_4\}$ unit within complex **2**. Hydrogen atoms, perchlorate anions and solvents are omitted for clarity.
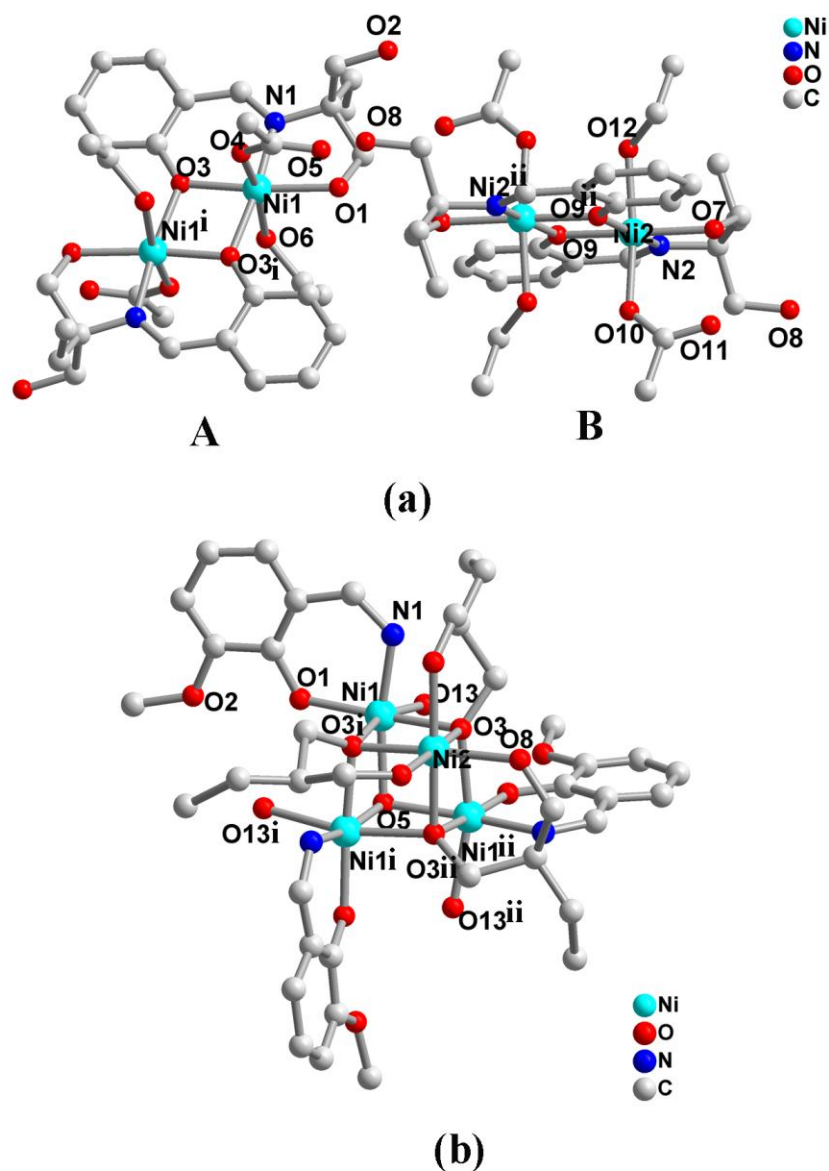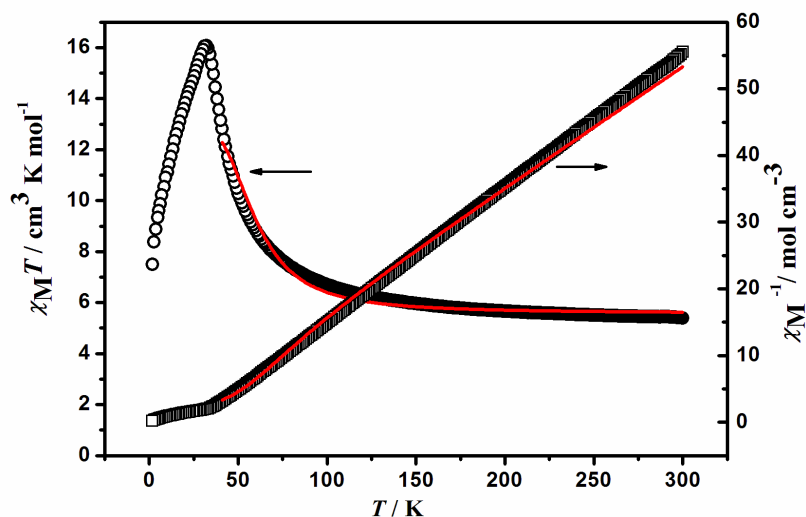
Figure 2. (a) Perspective view of binuclear in complex **3**. Hydrogen atoms are omitted for clarity, symmetry codes: i, -x, 1-y, 1-z; ii, -x,-y+2,-z. (b) Perspective view of complex **4**. Hydrogen atoms attached to carbon atoms and free water molecules are omitted for clarity. Symmetry codes: i, 1-z, x, 1-y; ii: y, 1-z, 1-x.

(a)

(b)

(c)
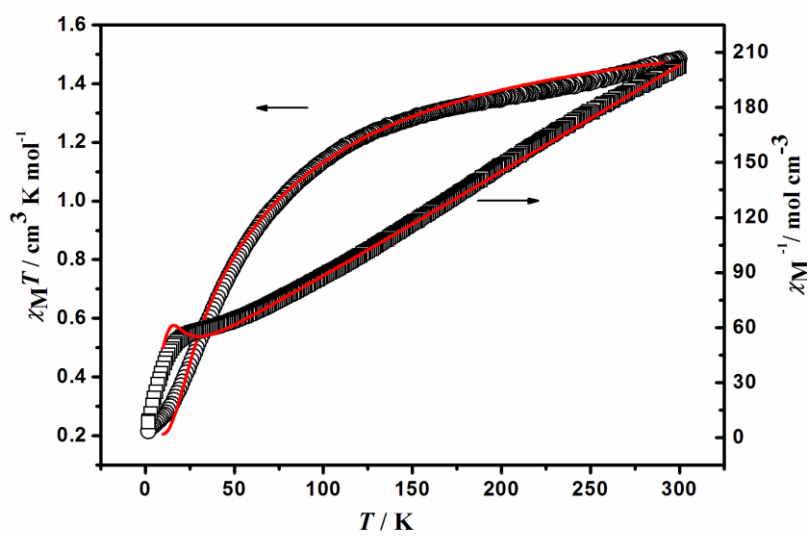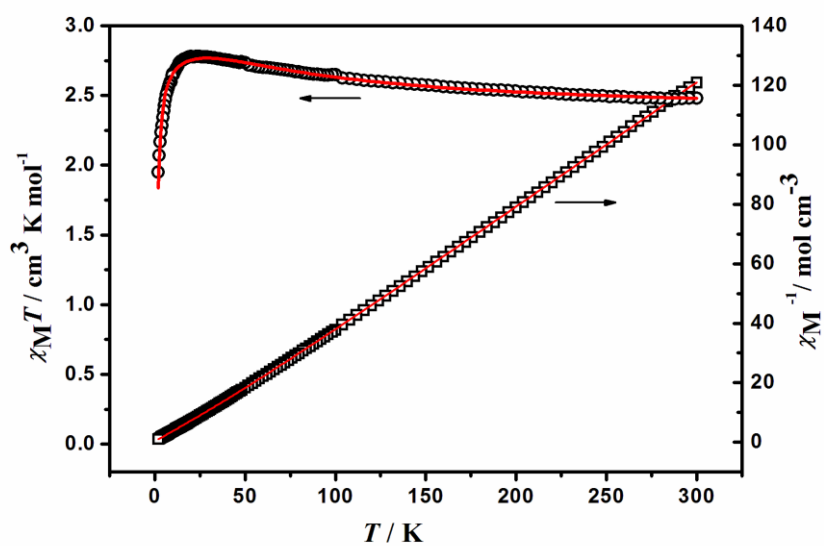
Figure 3. $\chi_M T$ and χ_M^{-1} vs. T plots for complexes **2**-**4** between 1.8 and 300 K in an applied field of 1kOe. The red solid lines represent the best-fit calculations.
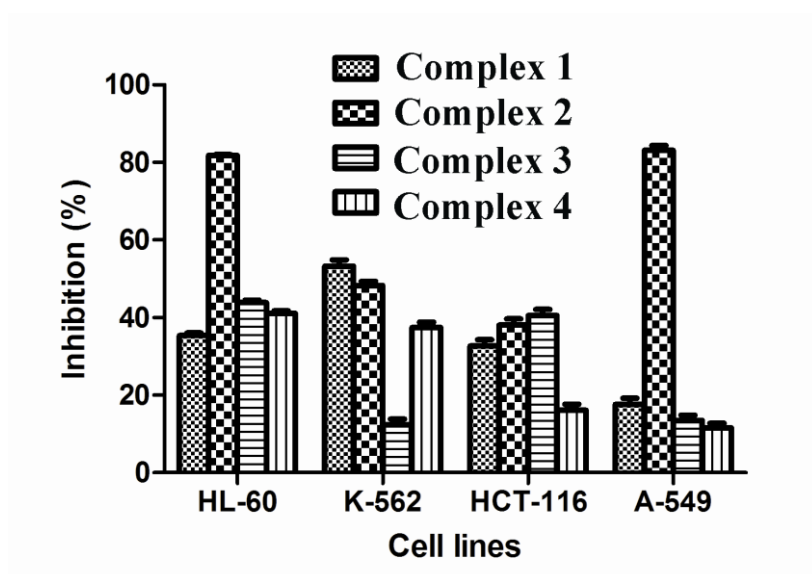
**Figure 4**.   Inhibition [%] of complexes **1**-**4** [dose level of 20.0 μg/mL] against human tumor cells.
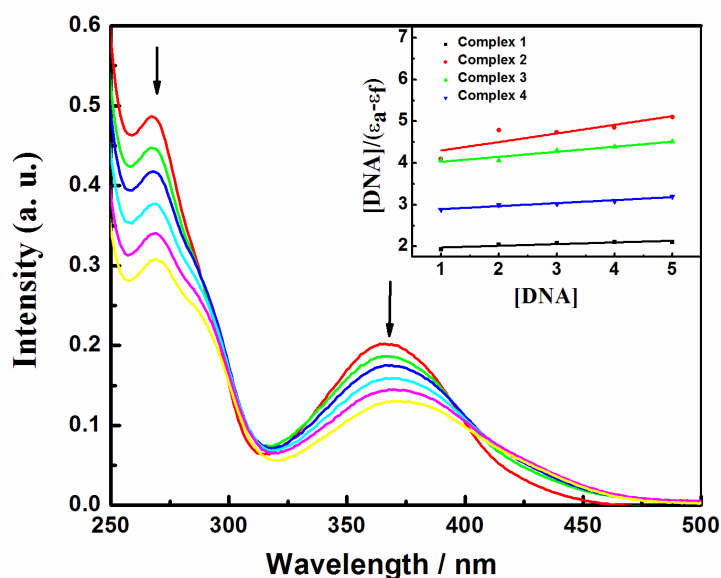
Figure 5. UV–vis absorption spectra of complex **3** in the absence and presence of CT-DNA, [VOL] $=10$ μM, from 1 to 6, [DNA] $=0$, 2, 4, 6, 8 and 10 μM, respectively; Inset: plots of $[DNA]/(\varepsilon_a-\varepsilon_f)$ vs. [DNA]. Arrows show the changes in absorbance with respect to an increase in the DNA concentration (Inset: a plot of $[DNA]/[\varepsilon_a-\varepsilon_f]$ versus [DNA] for complexes **1**-**4**).
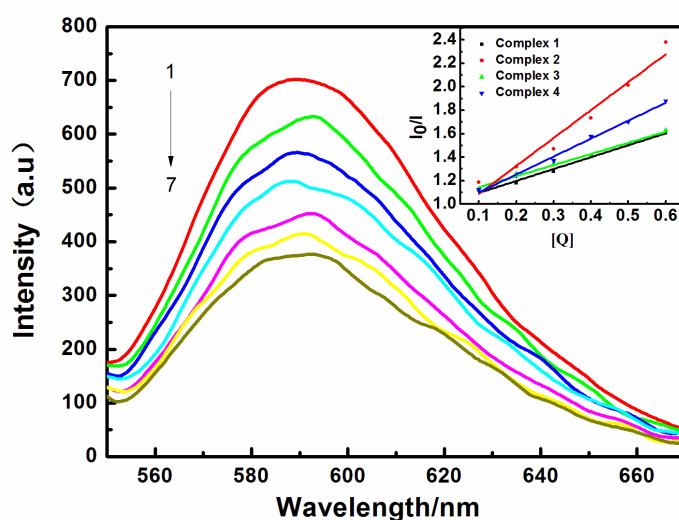

Figure 6. Effects of complex **4** on the fluorescent spectra of EB-DNA system ($\lambda ex=$ 258nm); $C_{DNA}= 30$ μM; $C_{EB}= 3$ μM; from 1 to 7, $C_{VOL} =0$, 6, 12, 18, 24, 30, 36 μM respectively (Inset: plot of I_0/I vs r ($r=C_{VOL}/ C_{DNA}$) for complexes **1**-**4**).
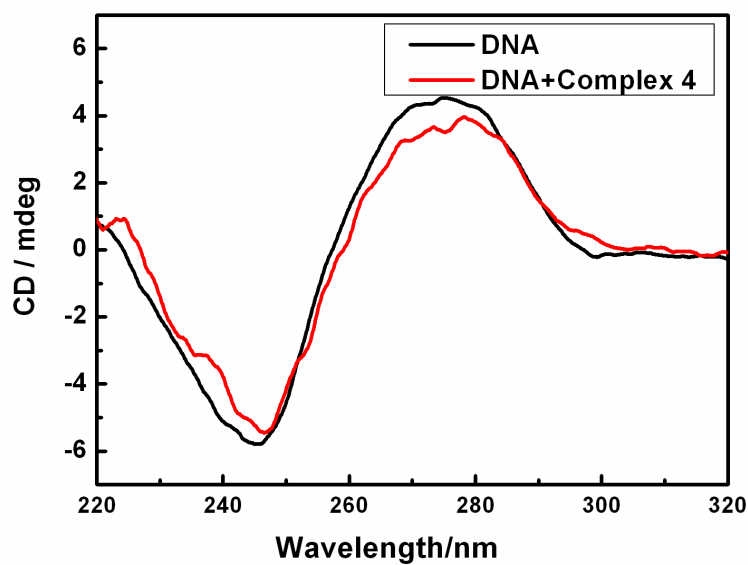
Figure 7. CD-spectra of CT-DNA in the absence and presence of complex **4**, [DNA] =100 μM, [VOL] = 0 and 40 μM, respectively.
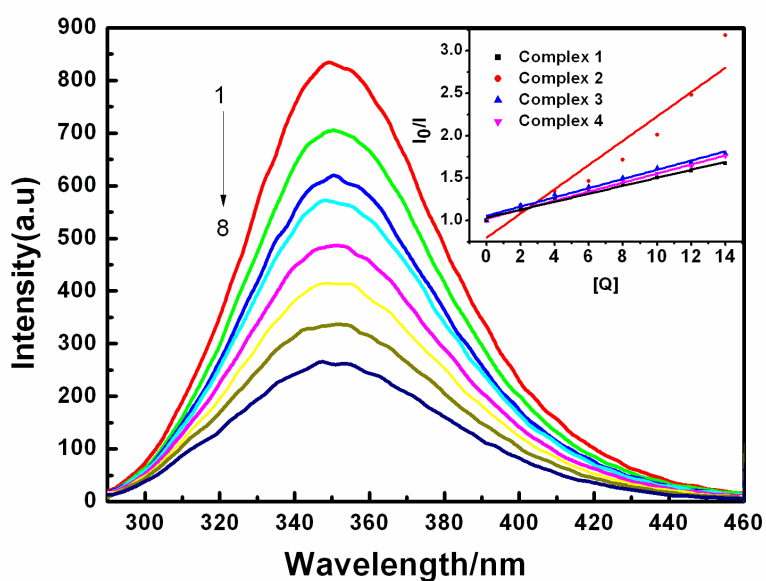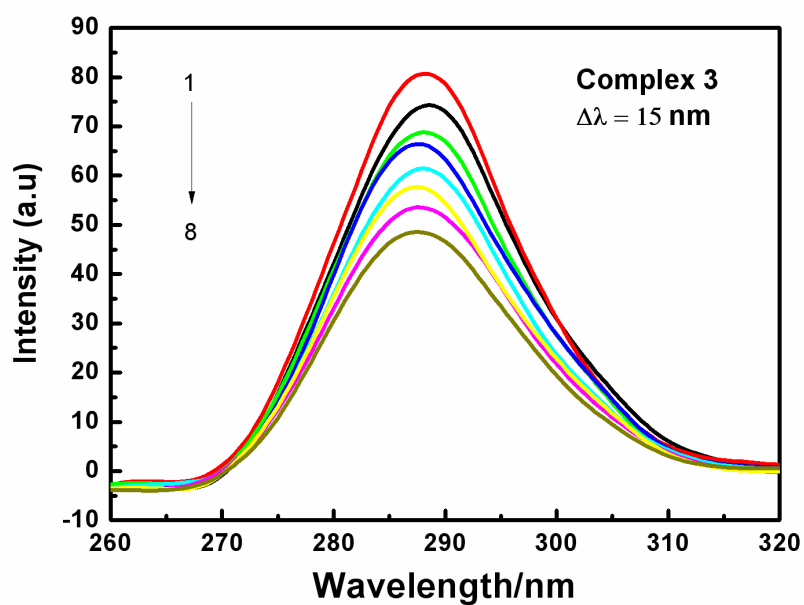

Figure 8. Fluorescence emission spectra of BSA in the absence and presence of complex **2**. [BSA] = 1 μM, [Complex] = 0, 2, 4, 6, 8, 10, 12, 14 μM, respectively; λ_{ex} = 280 nm (Inset: Plot of [Q] vs. I_0/I for complex **1**-**4**).
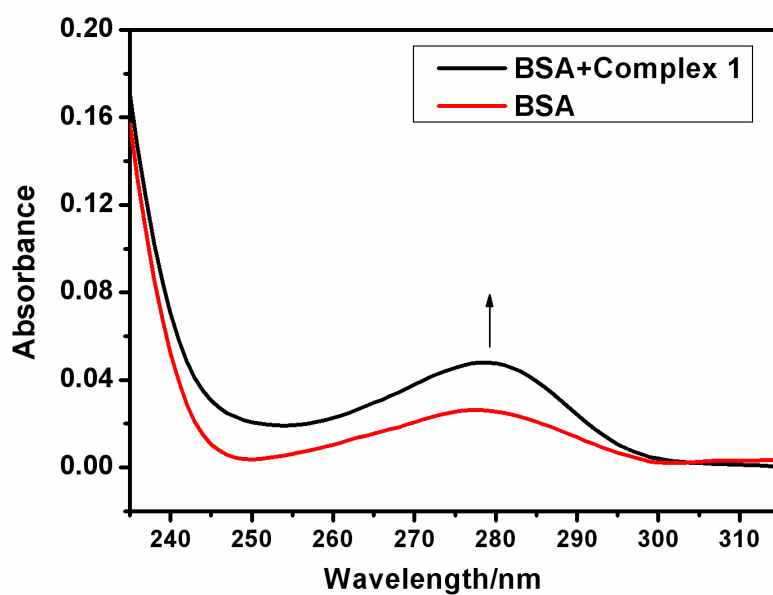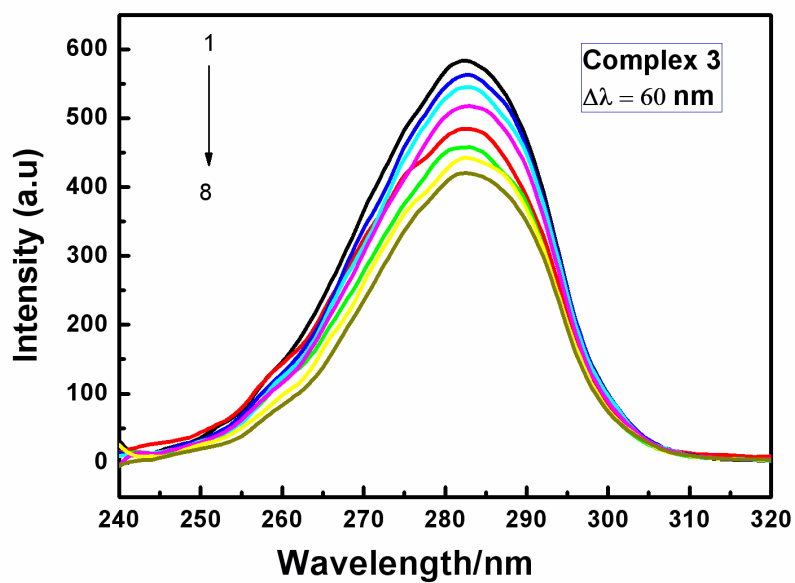
Figure 9. UV–vis absorption spectra of BSA in the absence and presence of the complex **1**. [BSA] = 1µM, [complex] = 0 and 1µM.
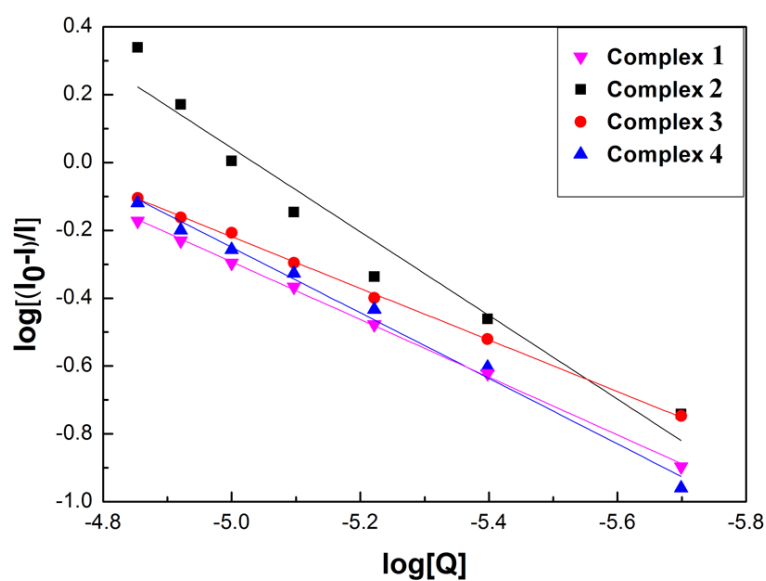
Figure 10. The plot of $\log[(I_0-I)/I]$ vs. $\log[Q]$.

(a)

(b)

Figure 11. Synchronous spectra of BSA as a function of concentration of the complex **3** with wavelength difference of $\Delta\lambda$ = 15 nm (a) and $\Delta\lambda$ = 60 nm (b).